Landscape structures regulate the contrasting response of recession along rainfall amounts

Jun-Yi Lee[1,2], Ci-Jian Yang[2,3], Tsung-Ren Peng[1], Tsung-Yu Lee[4], Jr-Chuan Huang[2]

[1]Department of Soil and Environmental Sciences, National Chung Hsing University, Taichung 402202, Taiwan
[2]Department of Geography, National Taiwan University, Taipei 106319, Taiwan
[3]German Research Centre for Geosciences (GFZ), Telegrafenberg, Potsdam 14473, Germany.
[4]Department of Geography, National Taiwan Normal University, Taipei 106209, Taiwan

Correspondence to: Jr-Chuan Huang(riverhuang@ntu.edu.tw)

Abstract. Streamflow recession discloses hydrological functioning, runoff dynamics, and storage status within catchments. Understanding recession response to landscape structures and rainstorms can be a guidance for assessing streamflow change under climate change. Yet, the documented response direction of recession is inconsistent and diverse. This study tested how landscape structures and rainstorms regulate the response direction. We derived a total of 291 pairs of recession coefficient, *a*, and nonlinearity, *b*, from power-law recession ($-dQ/dt = aQ^b$) over all 19 subtropical catchments with a broad rainfall spectrum. Results showed that the recession coefficient increases with the drainage density and L/G (the ratio of flow-path length to gradient), particularly in small catchments, indicating that catchments with the dense network more short-and-gentle hillslopes would result in high values of *a*. Apart from landscape structure, the *a* decreases with rainfall amount particularly in low L/G catchments. Probably because rainstorm facilitates connectivity in the saturated zones, which might conjoin more water from slow reservoirs and thus water drains slowly. Additionally, nonlinearity increases with rainfall amount in larger catchments but decreases in small catchments. The swing of response direction, which lies in the predominance between area and L/G, needs further clarification, particularly for regional recession assessment under climate changes. Incorrect response direction from landscape structure would lead to considerable bias inference.

1 Introduction

Streamflow recession, the falling segment of hydrograph, reflects a rainfall-runoff process and interaction among different runoffs during a rainstorm. Therefore, recession, associated with runoff paths within landscape, is particularly critical for baseflow estimation (Palmroth et al., 2010). Previous studies analyzed aggregated long-term data to retrieve recession parameters (e.g., Brutsaert and Nieber, 1977), but parameters from individual events can elucidate the recession characteristics of catchments (Jachens et al., 2020) and shed insight into the sensitivity of catchments to rainstorms, which is informative for water resource management. Therefore, recent studies have shifted to investigate recessions from individual events (Biswal and Nagesh Kumar, 2014; Jachens et al., 2020). A power-law relationship between streamflow declines (streamflow rate *Q* recesses with a timestep *t*) with streamflow rates ($-dQ/dt = \hat{a}Q^b$) can describe the recession characteristics at the catchment

scale (Brutsaert and Nieber, 1977). Parameter $\hat{a}$ approximates to the recession rate but is influenced by the unit of flow and b (see section 2.2.2), and parameter b represents the nonlinearity of storage. Recession parameters are often linked to the aquifer geometries, landscape, and spatial heterogeneity. Since the aquifer in various landscape units (e.g., hillslope, riparian, stream) exhibits different hydraulic properties and landscape structure, which presents the geometry of catchments and aggregates catchment hydraulic properties, apparently reflects various recession parameters. In theory, parameter $\hat{a}$ has a positive correlation with drainage density (total stream length/drainage area) and aquifer slopes but a negative correlation with aquifer depths, aquifer heterogeneity (of conductivity) (e.g., Brutsaert and Nieber, 1977; Rupp and Selker, 2006) and inter-hillslope heterogeneity (of celerity) (Harman et al., 2009). Parameter b increases with the number of streams (Biswal and Marani, 2010), the heterogeneity of the aquifer (Rupp and Selker, 2006) and the inter-hillslope (Harman et al., 2009), yet decrease with the total stream length (Biswal and Marani, 2010).

Theoretical works also have illustrated the temporal dependence of recession parameters on the groundwater table, recharge, and storage. From the perspective of temporal variability, parameter $\hat{a}$ is negatively correlated to the initial groundwater table (h_0) under unsaturated conditions and renders a slightly positive correlation under saturated conditions ($h_0 \geq B\tan\phi$, where B is aquifer length and is ϕ aquifer angle, Rupp and Selker, 2006). A large recharge rate also reduces parameter $\hat{a}$, particularly in homogenous catchments (Harman et al., 2009). On the other hand, hydraulic theories indicate that b decreases from 3.0 to 1.5 during the transition from early to late recession, as the groundwater is vertically sourced from different hydraulic properties in wet conditions (e.g., Rupp and Selker, 2006). The spatial heterogeneity theory demonstrates that b only slightly increases with the wet antecedent condition (Harman et al., 2009). However, the drainage network theory indicates that b increases/decreases with storage while reaches in downstream are contributed by more/fewer subsurface storages (Biswal and Nagesh Kumar, 2013). The various responses among theories implying the control of landscape structure and rainfall amount on recession in different regions should be improved.

The compilation of pervious empirical recession works (summarized in Table 1 and S1) demonstrated that most studies elucidated the recession parameters at long-term scale, and the relationships between recession parameters against landscape, landcover, and soil were inconsistent. For example, empirical recession parameters have inconsistent responses to several physiographic variables (drainage area, drainage density, water bodies coverage, and surface saturated conductivity), implying that different landscape regimes may have distinct recession responses. Additionally, most inter-event studies just analyzed the single parameter ($\hat{a}$) that decreases with the catchment wetness, which ignores the temporal variability of b. Only Biswal and Nagesh Kumar (2013) found the different directions of b response to peak flow, but which landscape variables would control the direction is still unclear. This compilation indicated that rare studies focused on the subtropical region and the variability of recession parameters at event scale.

This study investigated the recession parameters along with different magnitude of rainstorms (e.g. typhoons) on steep landscape in hope to identify the interactive role of rainfall and physiographic variables in recession. Specifically, we derived the recession coefficient and nonlinearity in 19 mountainous catchments (drainage area varies between 77–2,089 km^2) across Taiwan with multiyear records of hourly streamflow (291 events in total). Due to frequent tropical cyclones (alias: typhoon)

and mountainous landscapes, Taiwan's rivers lead to short water travel time and limit water retention capacity in catchments (Lee et al., 2020). Most typhoon rainwater falls in summer and elevates water level dramatically but diminishes quickly within 2-3 days (Huang et al., 2012). Here, the following questions are addressed: (1) What are the recession characteristics of typhoon events in subtropical mountainous catchments? (2) How do rainfall and landscape variables affect recession parameters in different landscape regimes? (3) In what way do landscape variables regulate the response of nonlinearity to rainfall? We documented the spatial patterns of recession parameters in Taiwan (Sect. 3) and then discussed how the recession behaviors change in different landscape settings (Sect. 4). Finally, we proposed a hypothesis: landscape structure could swing recession responses to rainstorms. Understanding the recession behaviors after typhoons are vital to water resource management, particularly when global warming likely increases the frequency and magnitude of flood and drought (Shiu et al., 2012; Huang et al., 2014).

2 Material and methods

2.1 Study area

Taiwan is geographically located at the juncture between the Eurasian and Philippine tectonic plates and climatologically located at the corridor of typhoons. The active mountain belt with frequent typhoons shapes steep and fractured landscapes with verdant forests. The mean annual rainfall is about 2,510 mm, and approx. 40% of annual rainfall is brought by typhoons in a few days. The lowest mean annual temperature is approx. 4℃ in montane regions and 22℃ in plain regions. In this mountainous island, the uplifting elevation (0–4,000 m) within a short horizontal distance (~75 km) shows the steep terrain (Huang et al., 2016). Specifically, the drainage area of most catchments is smaller than ~500 km^2 and stream lengths are less than ~55 km, indicating a short water travel time. The basic catchment descriptions of landscape variables could refer to Table S2. Land cover inventories from the Taiwan Ministry of the Interior (www.moi.gov.tw) were reclassified from the original 13 categories into three major categories; namely, water (C_W), forest (C_F), agriculture (C_A), and others for each catchment. The landscape metric described by the landscape variables were retrieved from the digital elevation model (DEM) with 20m resolution and referred to Table S2. The specific definitions of landscape variables are below: A is the drainage area [L^2]; DD is the drainage density [L/L^2] defined as the ratio of total stream length to drainage area; S_m is the gradient of mainstream [-]; HI is the hypsometric integral [-]; ELO is the basin elongation [-] defined as the ratio of the diameter of the circle (same area with the basin) to basin length. Notably, the flow-path is defined as the hillslope grid point following the surface flow direction toward the channel. Flow-path length (L) is the length of this path, and flow-path height (H) is the height difference along this path. G is the flow-path gradient [-]. These flow-path metrics and the L/G are often used in transit time studies (e.g., McGuire et al., 2005), helping to describe how landscape control on streamflow recession.

Streamflow in this steep mountainous island usually descends quickly after a considerable surge by a typhoon. Thus, hourly streamflow records are required to describe the entire streamflow recession since it only lasts a few days after peak. This study selected hourly streamflow records during 1986-2014 from the Taiwan Water Resource Agency (www.wra.gov.tw) and Tai-

Power Company (www.taipower.com.tw). Only the catchments without large water division infrastructures in the upstream area and the total rainfall larger than 30 mm were used to prevent human manipulation on streamflow and guarantee the discharge rise. Based on the criteria, nineteen catchments and 291 events were filtered for further recession analysis. Commensurate with the hourly streamflow, the hourly rainfall dataset from the Taiwan Central Weather Bureau (www.cwb.gov.tw) was introduced to Thiessen weighted method for areal rainfall estimation to the corresponding catchments. The rainfall period was defined as the elapse time from 6 hr before the rising flow to the peak flow. Collectively, a hydroclimate metric of rainstorm and streamflow presented total event rainfall, duration, average and maximum rainfall intensity, total streamflow, peak flow, and antecedent flow is shown in Table S3.

2.2 Recession analysis

As most analyses of hydrological processes do, the water balance equation is primarily described as Eq. (1):

$$\frac{dS}{dt} = P - E - Q \tag{1}$$

where S is the storage volume within a catchment (in units of volume [L^3] or depth [L]), and P, E, and Q are the rates of precipitation [L], evapotranspiration [L], and stream discharge [L^3/T] or [L/T], respectively. For solving the unknown storage, which cannot be measured directly, all terms should be identified. The formula $Q = mS^n$ with constant m and n (Vogel and Kroll, 1992), which follows Dupuit-Boussinesq equation, can be used to derive the relationship between storage and stream discharge. In this regard, S can be replaced by Q to infer the storage changes. During the recession period, P and E are relatively small compared to Q, and then the following equation is derived to represent the recession behaviors within a catchment.

$$-\frac{dQ}{dt} = nm^{\frac{1}{n}}Q^{\frac{2n-1}{n}} = \hat{a}Q^b \tag{2}$$

where $\hat{a}$ and b are constants derived from the Q-S relation. In this study, the stream discharge has been normalized by drainage area, and the unit of Q, $\hat{a}$ and b is [mm/h], [h^{-1} $(mm/h)^{1-b}$] and [-], respectively. This power-law form between $-dQ/dt$ and Q indicates that the rate of streamflow decline is highly relevant to Q during the recession and has been widely plotted as "recession plot" (Kirchner, 2009). This plot enables the analysis of streamflow recessions aggregatedly or event-independently and facilitates the derivation of storage–outflow relationships (Stölzle et al., 2013). Although the power-law formula and recession plot are widely used for describing the recession behavior, the retrieval procedures of recession extraction and parameter estimation are diverse due to different practical operations. For example, Stölzle et al. (2013) compared three extraction methods of recession segment in conjunction with their corresponding parameter estimations and all possible combinations. They found that recession characteristics like recession time ($1/a$) varied over 1–2 orders of magnitude, yet exponent b differed rather narrowly. Their results suggested that the recession characteristics derived with different procedures have only limited comparability and highlight the distinctiveness of individual procedures due to different purposes and philosophies. Dralle et al. (2017) also agreed with the above statement but they found that the relationship between $\hat{a}$ and

antecedent wetness were sensitive to the length of data. Despite the differences among the procedures, applying the same procedure to a regional extent still captures the recession characteristics. The following subsections present the procedures used for extraction and parameter estimation.

2.2.1 Recession segment extraction

In the extraction procedure, two concerns should be addressed: (1) distinguishing between the early and late recession stage, and (2) elimination of the unexpectedly positive increases in the recession. The early-stage (containing preceding storm and surface flow) and the late stage of recession (only dominated by base flow) are indistinguishable and usually determined subjectively based on different purposes. Some studies empirically excluded the early-stage recession from eliminating the influence of quick flow (e.g., Brutsaert, 2008; Vogel and Kroll, 1992). Some other studies used a threshold for the minimum length in extraction procedures from 2- to 10-days (e.g., Mendoza et al., 2003; Vogel and Kroll, 1992). For eliminating unexpectedly positive increases in recession, several approaches have been proposed as well, for example, smoothing the hydrograph (Vogel and Kroll, 1992), discarding the segment directly (Brutsaert, 2008; Kirchner, 2009), and breaking-and-rejoining the recession segments (Millares et al., 2009). Each strategy has its advantages and disadvantages; smoothing the hydrograph could not completely erase the bulge caused by precipitation; discarding the segment would lose part of recession events. Although breaking-and-rejoining the recession, too, disturbs the original streamflow records, the method maintains a better integral of a recession event.

The specific procedure of recession segment used in this study was described below. First, the recession evolution by typhoons is our main concern and thus we selected the whole recession segment from the peak flow of the individual rainstorm. The whole recession segment represents the mixing of quick and base flow interactively. Later, we screened and broke down the hydrograph as an abrupt bulge emerged, erased the positive streamflow increases, and concatenated the remaining segments. This elimination procedure is quite similar to the master recession curve on a long-term scale (Millares et al., 2009). Third, data points corresponding to extremely low streamflow ($Q < 0.1$ mm h^{-1}) or recession ($-dQ/dt < 0.01$ mm h^{-2}) were excluded, due to the undetectable change in recession. Forth, rainfall events with an unreasonable ratio of total flow to total rainfall ($Q/P > 1.1$ or $Q/P < 0.1$) were also excluded. Ultimately, a total of 298 rainstorms were selected for further parameter estimation.

2.2.2 Parameter fitting

Generally, the recession plot ($-dQ/dt$ vs Q) is widely used for estimation of recession parameters. But, several fitting methods have been proposed due to different philosophies in the literature. One is to fit with the lower envelope of the point-cloud (Brutsaert and Nieber, 1977) since the evapotranspiration effect in a recession would lead to a higher value of $-dQ/dt$. Taking the lower envelope can prevent the evapotranspiration effect. Another one is to fit with the entire point-cloud (Brutsaert, 2005; Vogel and Kroll, 1992) as subsoil heterogeneity may overshadow the evapotranspiration effect in larger or steeper catchments (Brutsaert, 2005). The other is to fit with the binned means weighted by the square of the standard error of each binned mean

(Kirchner, 2009) because the lower values of $-dQ/dt$ could be affected by the measurement errors in the streamflow observation. Recently, a virtual experiment study suggested to fit with individual recession segments in order to capture the recession characteristics and offer an opportunity for exploring the impacts of rainstorm properties. Because a group of data clouds (aggregated dataset) might result in underestimation of nonlinearity (Jachens et al., 2020). We, therefore, used each recession segment and fitted it with the power-law recession individually.

The specific parameter estimation for the retrieved recession segment was described below. Firstly, low-flow record correction: the same low flows appear frequently due to the detection limit of instruments and result in a series of zero value of $-dQ/dt$ which affects parameter estimation, particularly in b. We applied the exponential time step method (Roques et al., 2017) here to reduce the bias, in which the time step of the moving window exponentially increases along the recession. The extended sampling period could avoid the occurrence of zero values of $-dQ/dt$. Secondly, the decorrelation method: another important concern of parameter estimation in recession is the dependence between a and b, which blurs the interpretation of parameters. Therefore, we applied decorrelation method which assumes that the observed flow Q consists of a scale-free flow $\hat{Q}$ and a constant k ($Q = k\hat{Q}$). Thus, the power law formula can be rewritten as $-\mathrm{d}Q/\mathrm{d}t = ak^{b-1}\hat{Q}^b$, where a is scale-free recession coefficient [h^{-1}]. For correcting $\hat{a}$ to a, the observed flow Q was divided by a constant Q_0 (ideally equal to $1/k$, see detail in Dralle et al., 2015). After the decorrelation process, the number of catchments with a high correlation between a and b ($R^2 > 0.1$) decreased from 9 to 2. Finally, events with low goodness of fit ($R^2 < 0.5$) were discarded. Ultimately, each watershed had 5 to 26 events (total is 291, see Table S3) selected for exploring the landscape and rainstorm effects, of which events were not necessarily the same rainstorm.

3. Results

3.1. Recession parameters from individual and point-cloud fit

After proceeding with the mentioned analysis onto this dataset, we demonstrated the recession plots of W9, W5, and W8 in Fig. 2. The three catchments have distinct differences in landscape, particularly in drainage area and L/G (ratio of median flow-path length to median flow-path gradient to stream), see Table S2. Catchment W9 has a larger A and lower L/G, W5 has a lower A and lower L/G, and W8 has a smaller A, but higher L/G. In descending order, the ranking of median recession b is catchment W9 (2.34), W5 (1.96), and W8 (1.63). The point-cloud derived b are 1.45 (W9), 1.37(W5), and 0.88(W8), showing all point-cloud b are smaller than median ones (Fig. 2c). Notably, the nonlinearity decreases with the storm magnitude in W5 and W8, yet, the nonlinearity increases with the storm magnitude in W9 (Fig. 2b and 2c). The opposite responses of W9 and W5/W8 to storm magnitude coincide with the difference of drainage area. This apparent association will be explored further in the Discussion section.

Further, the frequency distributions of the fitted recession coefficient and nonlinearity of the total catchment-event records are shown in Figure 3a-b. Coefficient, a, ranges from 0.003 to 0.273 hr^{-1} with mean = 0.059 hr^{-1} and median = 0.047 hr^{-1}. The

large difference between the median and mean shows a right-skewed distribution. Nonlinearity, *b*, ranges from 0.90 to 4.39 with mean = 1.76 and median = 1.69. The small difference between the median and mean presents an asymmetric distribution of nonlinearity. Spatial patterns of recession coefficient and nonlinearity are illustrated in Fig. 3c-d. Generally, larger recession coefficients are located in the southwestern plain (Fig. 3c). Those plain catchments also have higher *L/G* values. Apart from this, no other distinct pattern can be found in other mountainous catchments. Conversely, the plot of recession nonlinearity presents a vague pattern (Fig. 3d), and no simple relationship could be found.

The recession parameters derived from individual segments and aggregated point-cloud data are illustrated in Fig. 4. The individual segment parameters which demonstrate the recession responses to each event present the holistic variation, whereas the point-cloud parameters that aggregate all recession segments in specific catchment are generally larger for the coefficient and smaller for the nonlinearity. Notably, when the drainage area is larger than 800 km^2 (W19), the coefficients from aggregated point-cloud get similar to the median of the individual segment. The coefficients are close to the upper limit from the aggregated point-cloud for small catchments, compared to W19. Besides, the deviations of aggregated point-cloud coefficients are distinctly larger in the small catchments. The median and interquartile of nonlinearity from individual segments are irrelative to drainage area, and the values from the aggregated point-cloud are consistently lower than that from individual segments. Distinct differences between coefficients and nonlinearities from the two fitting methods present the manipulation of fitting method, which results in the difficulty in comparison and inference. The details of the recession characteristics for each catchment can be referred to Table S4.

3.2 Recession parameters to event and landscape variables

The correlation coefficients of recession parameters to event-associated variables are shown in Fig. 5 and Table 1 to capture how hydrometric forcing affects recession. The total precipitation (P), duration (D), total streamflow (Q_{tot}), antecedent streamflow (Q_{ant}) and runoff coefficient (Q_{tot}/P) are negatively correlated to the recession coefficient, a. The average precipitation intensity (I_{avg}) and peak flow (Q_p), both of which represent the rainstorm magnitude, are not significant to a. As for initial conditions, simply defined as the 7-day antecedent precipitation, AP_{7day}, is not correlated to the a; other lengths of AP (3-, 5-, 14-, and 30-day) also show insignificant correlation to a. Notably, Q_{ant} is negatively correlated to a. Unlike recession coefficient, which strongly depends on the hydrometric variables, nonlinearity, b, is only positive to Q_{ant}. It indicated that higher antecedent flow could lead to higher nonlinearity. A little surprise is that the nonlinearity is statistically negative to peak flow (Q_p), presenting the nonlinearity decreases with rainstorm magnitude. To summarize from the view of the aggregated dataset, hydrometric forcing moderately controls the coefficient and only slightly involves nonlinearity.

On our 19 catchments, average height (H), length (L) and gradient (G) of flow-path are approx. 120 m, 252 m and 0.47, respectively (Table S2). Basically, those flow-path associated parameters are highly dependent. Thus, we used L/G, which has been proven highly correlated to water residence time (McGuire et al., 2005; Seybold et al., 2017), as a proxy presenting the interaction of landscape and climate, is approx. 951m. Forest is the dominant landscape, and the average forest coverage is

approx. 67.1% with a range between 11.8-92.1%. Notably, the catchments in the western plain are characterized by gentle gradients of flow-path, such as catchments W8, W9, W11, W12, W13, and W14. Due to the gentle landscape and higher *L/G*, agricultural activities are the dominant land cover in those catchments. The details of landscape variables could be referred to Table S1.

The correlations between recession parameters against event and landscape variables are illustrated in Fig. 5 and Table 1. Most landscape variables (*H*, *L*, *G*, *L*/*G*, *DD*, S_m, *HI*, C_W, C_F, and C_A) are significantly correlated to the coefficient, particularly for the flow-path-associated ones (*H*, *L*, *G*, *L/G*, and *DD*). The flow-path-associated variables, such as flow-path height (*H*), length (*L*), and gradient (*G*), are negatively correlated to the coefficients, but positive to *L/G* and *DD*. Besides, that coefficient increases with the decrease of S_m shows that quick recession occurs in a catchment with gentle gradient. In contrast, the coefficient increases with *HI*, showing a sharp recession in actively eroded catchments. Moreover, the coefficient increases with C_W (fraction of water body area) and C_A (fraction of agriculture area) and decreases with C_F (fraction of forest area). A catchment with more water bodies and agricultural lands leads to a faster recession, yet a catchment with more forest lands could reduce the recession coefficient. In short, most landscape variables are highly associated with the coefficient and only a few, such as *HI* and *A* are slightly negative to the nonlinearity. Yet, putting all catchments with various landscape features together may obscure the landscape control in recession coefficient and nonlinearity.

4. Discussion

4.1 Recession parameters in subtropical mountainous catchments

The range of recession coefficient from our 19 catchments is 0.010 to 0.290, comparable with values in the literature, for example, 0.012 to 0.230 for Swedish catchments (Bogaart et al., 2016) and 0.015 to 0.171 for USA watersheds (Biswal and Marani, 2010). Higher median recession coefficients are found in W8, W11, W12, and W14, where shorter- and steeper- flow paths, i.e., dense drainage networks, are the main landscape features. By contrast, catchments with longer- and gentle-flow paths, such as W7 and W15, have lower median recession coefficients. It indicates that landscape structure (e.g., drainage density and flow-path-associated variables) could affect the recession coefficient, as Table 2 shows. On the other hand, the median of recession nonlinearity, *b*, is approx. 1.6 (Fig. 3b) with a range of 0.6 to 3.0, which are also comparable with the ranges in the literature. For example, values of *b* from 0.5 to 2.1 could be found in 220 Swedish catchments with low flow data (Bogaart et al., 2016), 0.6 to 1.7 for 22 Taiwanese rivers derived from low-flow data (Yeh and Huang, 2019), and 1.5 to 3.2 for 67 USA watersheds with event data (Biswal and Marani, 2010). Non-linear storage-outflow relationship (b is not equal to 1.0) is prevalent for most catchments worldwide. In our cases, the highest and lowest median values of *b* are found in W7 and W19, respectively. Catchment W7 with high channel slope and flow-path gradient (Table S1), presents higher non-linear storage-outflow. W19, by contrast, has the similar landscape settings with W7, but has the lowest. Perhaps, other controlling factors, such as geological structure or land cover, might regulate the recession behavior (Tague and Grant, 2004).

Notably, a distinct systematic bias is found between the nonlinearity derived from individual segments and the aggregated point-cloud (Fig. 4). Smaller *b* value derived from the aggregated point-cloud than that from individual segments could be expected since the flood distribution is right-skewed; that is, large number of small cases with scarce extremes. Nonlinearity *b* derived from aggregated point-cloud is synthesized from all points, which could be altered either by the numerous small cases or the scarce extreme cases as fitting. The median from aggregated point-cloud is more or less like the way of the master recession curve. Jachens et al. (2020) indicated that the event properties (variation among inter-event, storm magnitude, and antecedent condition) strongly affect the parameter estimation. In this regard, it suggested that using the median from individual segments to represent the central tendency of a collection of recession segments (Dralle et al., 2017; Jachens et al., 2020), but the way to obtain the b is still goal-dependent (Sharma and Biswal, 2022).

4.2 Landscape structure controls the median of recession parameters

Landscape structure aggregates catchment hydraulic properties, embodying recession parameters conceivably. Therefore, recession behaviors in a catchment could be interpreted from two perspectives: hillslope hydraulics and inter-hillslope heterogeneity (Harman et al., 2009), both of which might be represented by the flow-path-associated variables (e.g., *H*, *L*, *G*, *L*/*G*, *DD* in Table 1) and drainage area. Notably, heterogeneity may increase with catchment area because of the possibility of including a wider range of subsurface conditions. Two studies, for example, investigated the recession behaviors in two small forested catchments (68 km^2 in Mahurangi, New Zealand, McMillan et al., 2014 and 41 ha in Panola Mountain Research Watershed, USA, Clark et al., 2009; Harman et al., 2009) and found that recession nonlinearity increases with drainage area because a larger area accommodates more possibility of superimposition of multiple linear reservoirs.

Correlation analysis elucidates that flow-path-associated variables (*H*, *L*, *G*, *L*/*G*, *DD*) only have a vague correlation with the recession nonlinearity (Fig. 6a). It might be explained by: first, some of our catchments are much larger than 500 km^2, which exceeds the extent of common rainstorms (usually less than 200 km^2). In those large catchments, the limited extent of rainstorm would not bring about a comprehensive recession response in the outflow hydrograph (Huang et al., 2012). Second, drainage area cannot reflect the unknown number of aquifers (Ajami et al., 2011). Moreover, Karlsen et al. (2019) argued that the dependence of landscape variables would change with streamflow rate. Specifically, the variable, *H*, dominates the nonlinearity during high flow, whereas the variable, drainage area, gains more importance during low flows. The relationship between flow-path-associated variables and drainage area against recession needs to be further examined in our catchments.

4.2.1 Landscape structure to recession coefficient, *a*

The significance of landscape variables might be altered by drainage area, which might result in an opposite recession response. Further, in our cases, catchment area could not solely and significantly explain the recession behaviors (Fig. 6a). The flow-path-associated variables were tried to correlate with drainage area and an inverse relationship between L/G ratio against drainage area emerged surprisingly (Fig. 6b). The *L*/*G* ratio, a measure of the distribution of flow-path length over gradient at a catchment scale (McGuire et al., 2005), is highly correlated to *DD* and the topographic wetness index (Beven and Kirkby,

1979). Therefore, *L/G* is apt to present the hillslope hydraulics at a catchment scale. In Fig. 6b, all catchments could be simply classified into three types: type A is large catchments (area > 500 km^2), B is small catchments with low L/G, and C is small catchments with high L/G. The flow-path-associated variables (*H*, *L*, *L*/*G*, and DD) are re-applied onto the recession parameters according to this classification (Fig. 7). As expected, the recession coefficients correlate with the flow-path-associated variables. *H* is directly linked to the water table depth under the relatively homogeneous hillslopes. Hence, steeper hillslope corresponds to permeable soils with higher *H*, leading to a deeper and longer groundwater flow system and slower drainage (Karlsen et al., 2019). The high *DD* and short *L* lead to a higher recession coefficient due to shorter flow paths. Additionally, McGuire et al. (2005) demonstrated isotopic evidence to prove that the transit time increases with *L* in Oregon, USA. In our case, both *DD* and *L/G* (Fig. 7a-c) confirm the documented relations. Catchments with high *DD* or *L/G*, which represent a denser stream network or short-and-gentle hillslopes, have a higher recession coefficient.

Appeal to existing theories, flow-path variables could be regarded as the aggregation of aquifers with various geometries, or vertical heterogeneity of aquifer (Rupp and Selker, 2006). Flow-path variables L, H, G can be the proxy of $B\cos\phi$, $B\sin\phi+D\cos\phi$, and $D/B+\tan\phi$, respectively. Large *B* and $\tan\phi$ aquifers have a small coefficient *a* (Fig. 3 in Rupp and Selker, 2006, where B, D, ϕ indicate the length, depth, and slope of the aquifer, respectively). Our inverse relationship between *H* and *a* confirms that the hydraulic parameters vary markedly with depth (Rupp and Selker, 2006).

4.2.2 Landscape structure to recession nonlinearity, *b*

The recession nonlinearity conditionally responds to landscape structure (Fig. 7e-7h). If Type A catchments (large area with low *L/G*, gray solid dots in Fig. 7) are excluded, all flow-path-associated variables become statistically significant with nonlinearity. The positive relationship of *b* with *H* and *L* indicates that steeper and rougher hillslope present non-linear recession behaviour. With the increase of flow-path, subsurface runoff has more chances of flowing through various blocks (e.g., temporarily perched groundwater). The two composite indices, *DD* and *L*/*G*, are negatively related to the value of *b* (Fig. 7g-h), perhaps because that short-and-gentle hillslopes lead to a larger saturation area (Bogaart et al., 2016; Sayama et al., 2011). The expansion of saturation area indicates the whole subsurface is getting saturated and connected and thus reduces heterogeneity. It suggested that *L/G* ratio affects the nonlinearity significantly for small catchments; however, it is not valid for our large catchments, which necessitates further theory development.

4.3 Rainfall amount controls the variation of recession parameters

Recession behavior is a convolutional response starting as rainfall falling within catchments. Thus, we separately examined the recession parameters against hydrometric variables for the three catchment types to rule out the influences (Fig. 8). Two significant findings are: (1) the recession coefficient decreases with the rainfall amount in all types; (2) the recession nonlinearity shows opposite responses in Type A and B (Type C is statistically insignificant). The parameter, *b*, in

heterogeneity-dominated or hydraulics-dominated catchments would increase or decrease with rainfall amount, respectively. The contrasting recession responses are further discussed in the following two sections.

4.3.1 Rainfall amount on recession coefficient, *a*

Several empirical studies found a positive or independent relationship between coefficient, *a* and streamflow; for example, Santos et al. (2019) found that higher streamflow has a larger *a*, reflecting a quick recession in Switzerland catchments. In Sweden, annual rainfall variation might be independent of the *a* (Bogaart et al., 2016). Harman's virtual experiments demonstrated that the recession coefficient is determined by the tension between the recharge rate and the spatial heterogeneity of storage and flow velocity (Hamann et al., 2009). In our three catchment types, recession coefficients decrease with rainfall amount (Fig. 8a-c). It may infer that the huge rainfall brought by typhoons may overwhelm the effect of flow velocity, resulting in a slower recession in large rainstorms. Interestingly, Type C has a higher intercept of the rainfall-*a* relationship like the theorical curve of $h_0/D=1$ (Rupp and Selker, 2006), suggesting that the lower H of type C tends to be saturated and have a quick recession.

4.3.2 Opposite control of rainfall on recession nonlinearity, *b*

The variation of recession nonlinearity among events is divergent. Some studies concluded that nonlinearity, *b*, is controlled by landscape structure and is static or is insensitive to rainfall (Biswal and Marani, 2010; Brutsaert and Nieber, 1977; Dralle et al., 2017). In other studies, nonlinearity, *b*, decreases with streamflow rate on different temporal scales (Shaw and Riha, 2012; Karlsen et al., 2019; Santos et al., 2019). Although some studies even argued that the nonlinearity can change over the course of an event (Rupp and Selker, 2006; Luo et al., 2018), this study treated b as a constant and the inter-event variability is discussed as the following. In our study, nonlinearity *b* presents a positive, flat, negative relationship with rainfall in Type A, B, and C catchments, respectively (Fig. 8d-f). A possible interpretation is that the short-and-gentle catchments (Type C catchments) have a wide range of contributing area, which expands with rainfall quickly. The pervasive saturation overland flow reduces the nonlinearity of recession. With the connection of saturated zones, the large storms can activate different draining sources, mixing them downstream and result in the decrease of b (as Type C demonstrated). On the contrary, the nonlinearity, *b*, increases with the rainfall amount in Type A catchments. In large and heterogeneous catchments, the expansion of contributing area is more unsteady and complicated, and thus the nonlinearity increases with rainfall amount. The nonlinearity increases with the heterogeneity within a large catchment (Harman et al., 2009). The contrasting response of *b* to rainfall was only found in Biswal and Nagesh Kumar (2013), which attributed to the change in subsurface flow contributions along the channel that affect the direction response of *b*. Our study revealed that landscape structure and rainfall amount dominate the direction and magnitude of recession response, respectively. Future research direction could further consider different landscape structures into modelling the intra-event variation of *b*.

4.4 Landscape structure regulates recession patterns

The above two sections elucidate the role of landscape rainfall amount in recession behaviors. Thus, a hypothesis which demonstrates the interactive regulation of landscape structure and rainfall amount on recession nonlinearity is introduced (Fig. 9). Landscape structure is considered from two dimensions in terms of spatial heterogeneity and hillslope hydraulic, which are, respectively, represented by drainage area and L/G. While the drainage area might correlate to the number of perched storages within the catchments, the *L/G* featured by short-and-gentle hillslope indicates that the size of contributing area associated with runoff generation.

Along spatial heterogeneity dimension (from Type B to A, with increasing drainage area), additional perched storages respond increasingly with rainfall amount and thus enhance the recession nonlinearity. Perched storages are inclined to occur where the hydrological conductivity abruptly decreases due to heterogeneous soil properties or geological structure. The existence of perched storages was found in an experimental forested catchment in Taiwan by an intensive pore water monitoring scheme (Liang, 2020). Large catchments might have more perched storages, and consequently uneven spatial rainfall activate perched storages locally, and thus, the nonlinearity increases. On the other hand, along the L/G dimension (from Type B to C), the accumulated rainfall expands saturation zone quickly, which prefers the generation of saturation excess overland flow. With the increase of *L/G*, the runoff generation varies from subsurface runoff to overall saturation excess overland flow, and thus decreases nonlinearity.

5. Summary

Streamflow recession, which reflects the rainfall-runoff process after rainstorms, is crucial for baseflow estimation and assessment. This study investigated the recession responses to landscape structure and rainfall amount through power-law recession from 291 catchment events. Despite the power-law equation being widely used, the procedure of parameter estimation is diverse and of considerable inconsistency. For example, the selection of recession segments predominates the coefficient and nonlinearity significantly and leads to controversy, which makes the inter-comparison among studies complicated and delivers biased inference.

In our cases, landscape structure, mainly *DD* or *L/G*, and rainfall amount play dominant roles in estimating recession coefficient. The coefficient increases with the increase of *DD* or *L/G*, indicating catchments with dense networks or more short-and-gentle hillslopes would lead to a higher coefficient. Surprisingly, it decreases with rainfall amount; probably the large rainfall develops saturated zones connectivity, resulting in more water from slow reservoirs and drained slowly. The diverse response direction of nonlinearity likely depends on spatial heterogeneity (drainage area) and L/G, respectively. The more heterogeneous catchments give rise to the increase in the recession nonlinearity. On the contrary, catchments with gentle slopes could expand contributing area easily, and then generate saturation overland flow pervasively and thus reduce recession nonlinearity. Conjointly, our hypothesis presents an interactive regulation of landscape structure and rainfall amount to recession. In sum, landscape structure which has different preferences of recession mechanism, and the rainfall amount tunes

the magnitude of recession nonlinearity apparently. If the hypothesis is valid, two challenges should be addressed further. First, the alteration of response direction in the predominance between spatial heterogeneity and L/G necessitates theoretical validation further. Clarifying which factors could present the spatial heterogeneity and hillslope hydraulics is also an arduous task but is crucial for recession estimation. Second, the determination of response direction is crucial to the regional recession assessment, particularly for climatic scenarios. An incorrect direction would strongly affect the inference. Validating the landscape structure control in different regions would aid in completing the understating of recession variations.

Data availability. Hourly streamflow data can be obtained from Taiwan Water Resource Agency and Tai-Power company. The authors declare that data supporting the findings of this study are accessible from the article and its supplementary materials.

Author contributions. Conceptualization and Methodology: JYL and JCH. Data Curation and Validation: TYL. Formal analysis: JYL and CJY. Investigation and Writing – Original Draft: JYL. Writing – Review and Editing: JCH and TRP.

Competing interests. The authors claim no potential competing interests

Acknowledgements. This research was funded by the Ministry of Science and Technology, Taiwan (110-2811-M-005-509, and 109-2811-B-002-631) and the NTU Research Center for Future Earth (107L901004). J. Y. Lee and C. J. Yang was supported by the grants from Ministry of Science and Technology, Taiwan (110-2811-M-005-521, 110-2917-I-564-009).

References

Ajami, H., Troch, P. A., Maddock III, T., Meixner, T., and Eastoe, C.: Quantifying mountain block recharge by means of catchment-scale storage-discharge relationships, Water Resour. Res., 47, W04504, https://doi.org/10.1029/2010WR009598, 2011.

Beven, K. J. and Kirkby, M. J.: A physically based, variable contributing area model of basin hydrology, Hydrol. Sci. J., 24, 43–69, https://doi.org/10.1080/02626667909491834, 1979.

Biswal, B. and Marani, M.: Geomorphological origin of recession curves, Geophys. Res. Lett., 37, L24403, https://doi.org/10.1029/2010GL045415, 2010.

Biswal, B., and Nagesh Kumar, D.: A general geomorphological recession flow model for river basins. Water Resour. Res., 49(8), 4900-4906, https://doi.org/10.1002/wrcr.20379, 2013.

Biswal, B. and Nagesh Kumar, D.: Study of dynamic behaviour of recession curves, Hydrol. Process., 28, 784–792, https://doi.org/10.1002/hyp.9604, 2014.

Bogaart, P. W., Van Der Velde, Y., Lyon, S. W., and Dekker, S. C.: Streamflow recession patterns can help unravel the role of climate and humans in landscape co-evolution, Hydrol. Earth Syst. Sci., 20, 1413–1432, https://doi.org/10.5194/hess-20-1413-2016, 2016.

Brutsaert, W.: Hydrology: an introduction, Cambridge university press, https://doi.org/10.1017/CBO9780511808470, 2005.

Brutsaert, W.: Long-term groundwater storage trends estimated from streamflow records: Climatic perspective, Water Resour. Res., 44, W02409, https://doi.org/10.1029/2007WR006518, 2008.

Brutsaert, W. and Nieber, J. L.: Regionalized drought flow hydrographs from a mature glaciated plateau, Water Resour. Res., 13, 637–643, https://doi.org/10.1029/WR013i003p00637, 1977.

Clark, M. P., Rupp, D. E., Woods, R. A., Tromp-van Meerveld, H., Peters, N., and Freer, J.: Consistency between hydrological models and field observations: linking processes at the hillslope scale to hydrological responses at the watershed scale, Hydrol. Process. Int. J., 23, 311–319, https://doi.org/10.1002/hyp.7154, 2009.

Dralle, D., Karst, N., and Thompson, S. E.: a, b careful: The challenge of scale invariance for comparative analyses in power law models of the streamflow recession. Geophys. Res. Lett., 42(21), 9285-9293, https://doi.org/10.1002/2015GL066007, 2015.

Dralle, D. N., Karst, N. J., Charalampous, K., Veenstra, A., and Thompson, S. E.: Event-scale power law recession analysis: quantifying methodological uncertainty, Hydrol. Earth Syst. Sci., 21, 65–81, https://doi.org/10.5194/hess-21-65-2017, 2017.

Harman, C. J., Sivapalan, M., and Kumar, P.: Power law catchment-scale recessions arising from heterogeneous linear small-scale dynamics, Water Resour. Res., 45, W09404, https://doi.org/10.1029/2008WR007392, 2009.

Huang, J.-C., Yu, C.-K., Lee, J.-Y., Cheng, L.-W., Lee, T.-Y., and Kao, S.-J.: Linking typhoon tracks and spatial rainfall patterns for improving flood lead time predictions over a mesoscale mountainous watershed, Water Resour. Res., 48, W09540, https://doi.org/10.1029/2011WR011508, 2012.

Huang, J.-C., Lee, T.-Y., and Lee, J.-Y.: Observed magnified runoff response to rainfall intensification under global warming, Environmental Research Letters, 9, 034008, https://doi.org/10.1088/1748-9326/9/3/034008, 2014.

Huang, J.-C., Lee, T.-Y., Lin, T.-C., Hein, T., Lee, L.-C., Shih, Y.-T., Kao, S.-J., Shiah, F.-K., and Lin, N.-H.: Effects of different N sources on riverine DIN export and retention in a subtropical high-standing island, Taiwan, Biogeosciences, 13, 1787–1800, https://doi.org/10.5194/bg-13-1787-2016, 2016.

Jachens, E. R., Rupp, D. E., Roques, C., and Selker, J. S.: Recession analysis revisited: impacts of climate on parameter estimation, Hydrol. Earth Syst. Sci., 24, 1159–1170, https://doi.org/10.5194/hess-24-1159-2020, 2020.

Karlsen, R. H., Bishop, K., Grabs, T., Ottosson-Löfvenius, M., Laudon, H., and Seibert, J.: The role of landscape properties, storage and evapotranspiration on variability in streamflow recessions in a boreal catchment, J. Hydrol., 570, 315–328, https://doi.org/10.1016/j.jhydrol.2018.12.065, 2019.

Kirchner, J. W.: Catchments as simple dynamical systems: Catchment characterization, rainfall-runoff modeling, and doing hydrology backward, Water Resour. Res., 45, W02429, https://doi.org/10.1029/2008WR006912, 2009.

Lee, J.-Y., Shih, Y.-T., Lan, C.-Y., Lee, T.-Y., Peng, T.-R., Lee, C.-T., Huang, J.-C.: Rainstorm Magnitude Likely Regulates Event Water Fraction and Its Transit Time in Mesoscale Mountainous Catchments: Implication for Modelling Parameterization. Water, 12, 1169, https://doi.org/10.3390/w12041169, 2020.

Liang, W. L.: Dynamics of pore water pressure at the soil–bedrock interface recorded during a rainfall-induced shallow landslide in a steep natural forested headwater catchment, Taiwan. J. Hydrol., 587, 125003, https://doi.org/10.1016/j.jhydrol.2020.125003, 2020.

Luo, Z., Shen, C., Kong, J., Hua, G., Gao, X., Zhao, Z., Zhao, H., and Li, L.: Effects of unsaturated flow on hillslope recession characteristics. Water Resour. Res., 54(3), 2037-2056, https://doi.org/10.1002/2017WR022257, 2018

McGuire, K., McDonnell, J. J., Weiler, M., Kendall, C., McGlynn, B., Welker, J., and Seibert, J.: The role of topography on catchment-scale water residence time, Water Resour. Res., 41, W05002, https://doi.org/10.1029/2004WR003657, 2005.

McMillan, H., Gueguen, M., Grimon, E., Woods, R., Clark, M., and Rupp, D. E.: Spatial variability of hydrological processes and model structure diagnostics in a 50 km^2 catchment, Hydrol. Process., 28, 4896–4913, https://doi.org/10.1002/hyp.9988, 2014.

Mendoza, G. F., Steenhuis, T. S., Walter, M. T., and Parlange, J.-Y.: Estimating basin-wide hydraulic parameters of a semi-arid mountainous watershed by recession-flow analysis, J. Hydrol., 279, 57–69, https://doi.org/10.1016/S0022-1694(03)00174-4, 2003.

Millares, A., Polo, M. J., and Losada, M. A.: The hydrological response of baseflow in fractured mountain areas, Hydrol. Earth Syst. Sci., 13, 1261–1271, https://doi.org/10.5194/hess-13-1261-2009, 2009.

Palmroth, S., Katul, G. G., Hui, D., McCarthy, H. R., Jackson, R. B., and Oren, R.: Estimation of long-term basin scale evapotranspiration from streamflow time series, Water Resour. Res., 46, W10512, https://doi.org/10.1029/2009WR008838, 2010.

Roques, C., Rupp, D. E., and Selker, J. S.: Improved streamflow recession parameter estimation with attention to calculation of− dQ/dt. Adv. Water Resour. , 108, 29-43, https://doi.org/10.1016/j.advwatres.2017.07.013, 2017

Rupp, D. E., and Selker, J. S.: On the use of the Boussinesq equation for interpreting recession hydrographs from sloping aquifers. Water Resour. Res., 42(12), https://doi.org/10.1029/2006WR005080, 2006.

Santos, A. C., Portela, M. M., Rinaldo, A., and Schaefli, B.: Estimation of streamflow recession parameters: New insights from an analytic streamflow distribution model, Hydrol. Process., 33, 1595–1609, https://doi.org/10.1002/hyp.13425, 2019.

Sayama, T., McDonnell, J. J., Dhakal, A., and Sullivan, K.: How much water can a watershed store?, Hydrol. Process., 25, 3899–3908, https://doi.org/10.1002/hyp.8288, 2011.

Shaw, S. B. and Riha, S. J.: Examining individual recession events instead of a data cloud: Using a modified interpretation of dQ/dt–Q streamflow recession in glaciated watersheds to better inform models of low flow, J. Hydrol., 434, 46–54, https://doi.org/10.1016/j.jhydrol.2012.02.034, 2012.

Shiu, C., Liu, S. C., Fu, C., Dai, A., and Sun, Y.: How much do precipitation extremes change in a warming climate?, Geophys. Res. Lett., 39, L17707, https://doi.org/10.1029/2012GL052762, 2012.

Stölzle, M., Stahl, K., and Weiler, M.: Are streamflow recession characteristics really characteristic?, Hydrol. Earth Syst. Sci., 17, 817–828, https://doi.org/10.5194/hess-17-817-2013, 2013.

Tague, C. and Grant, G. E.: A geological framework for interpreting the low-flow regimes of Cascade streams, Willamette River Basin, Oregon, Water Resour. Res., 40, W04303, https://doi.org/10.1029/2003WR002629, 2004.

Vogel, R. M. and Kroll, C. N.: Regional geohydrologic-geomorphic relationships for the estimation of low-flow statistics, Water Resour. Res., 28, 2451–2458, https://doi.org/10.1029/92WR01007, 1992.

Yeh, H. and Huang, C.: Evaluation of basin storage–discharge sensitivity in Taiwan using low-flow recession analysis, Hydrol. Process., 33, 1434–1447, https://doi.org/10.1002/hyp.13411, 2019.

Seybold, H., Rothman, D. H., and Kirchner, J. W.: Climate's watermark in the geometry of stream networks. Geophysical Research Letters, 44(5), 2272-2280, https://doi.org/10.1002/2016GL072089, 2017.

Table 1: Summary of empirical recession studies that investigated the dependence of recession parameters on environmental factors. Shade blue, red, and grey represent positive, negative, and no correlation with factors, respectively. The label of number indicates the reference number in Table S1.

Factor	Centrality of recession		Temporal variability of recession					
	Long-term		Inter-annual		Inter-seasonal		Inter-event	
	â	b	â	b	â	b	â	b
Climate/Moisture								
Annual rainfall	1, 21	1	21	21				
		21						
Maximum monthly rainfall		2						
Antecedent flow					4, 5		5, 13, **22**	
Peak flow							8	19
							6	19
								8
Flow rate after peak							5, 6, 9	23
							23	
Total storage change						11		
Water table elevation					**3**	3		
Saturated area					**3**	3		
60 cm soil moisture					**3**	3		
Baseflow	1							
Evapotranspiration	1, 21	1			**3**, 12, 24	24		
		21				3		
Aridity index	16, 17, 21	15, 16, 17, 21						
Mean relative humidity		2						
Landscape								
Drainage area	10, 16, 20	1, 7, 16, 18, 24						
	1	20						
Long shape of catchment	10							
Flow path height		24						
Mean elevation		2						
Standard deviation of elevation		2						
Catchment slope	17, 24	2, 17, 24						
Coefficient of variation of slope	16	16						
Topographic wetness index		2						
Drainage density	14	14						
	10							

Subsurface flow contact time		2			
Landcover					
Reforestation			21	21	
Water management			21	21	
Plateaus coverage		15			
Young volcano rock coverage	14	14			
Forest coverage	18				
Water bodies coverage	21	16, 21, 24			
	16				
Flood attenuation due to lakes	1	1			
Soil					
Soil depth		24			
Surface hydraulic conductivity	17	21			
	18	17			
Field capacity	16	16			
Moderate infiltration rates soil		2			
Slow infiltration rates soil		2			
Playas with impermeable soils		15			
Organic matter content		2			

Table 2: Spearman correlation coefficients between logarithmic hydrometric characteristics and recession characteristics for all catchment-events (n = 291). Values in bold are statistically significant with the 99% level of confidence (p-value< 0.01).

Variable	Meaning	a [hr^{-1}]	b [-]
Hydrometric			
AP_{7day} [mm]	7-day antecedent precipitation	-0.080	0.010
P [mm]	Total precipitation	**-0.524**	-0.083
D [hr]	Duration of precipitation	**-0.432**	-0.054
I_{avg} [mm hr^{-1}]	Averaged precipitation intensity	**-0.257**	-0.026
Q_{tot} [mm]	Total streamflow	**-0.609**	-0.154
Q_{ant} [mm]	Antecedent streamflow	**-0.339**	**0.266**
Q_p [mm]	Peak flow	**-0.247**	**-0.228**
Q_{tot}/P [-]	Runoff coefficient	**-0.337**	-0.097
Landscape			
H [m]	Flow-path height	**-0.491**	**0.224**
L [m]	Flow-path length	**-0.520**	**0.302**
G [-]	Flow-path gradient	**-0.453**	0.189
L/G [m]	Ratio of flow-path length to gradient	**0.470**	-0.181
A [km^2]	Drainage area	0.040	-0.095
DD [km]	Drainage density	**0.420**	-0.217
S_m [%]	Gradient of mainstream	**-0.318**	**0.229**
HI [-]	Hypsometric integral	**-0.498**	**0.226**
ELO [-]	Basin elongation	-0.209	**0.319**
C_W [%]	Land cover - water bodies	**0.330**	-0.147
C_F [%]	Land cover - forest	**-0.281**	0.140
C_A [%]	Land cover - agriculture	**0.268**	-0.059

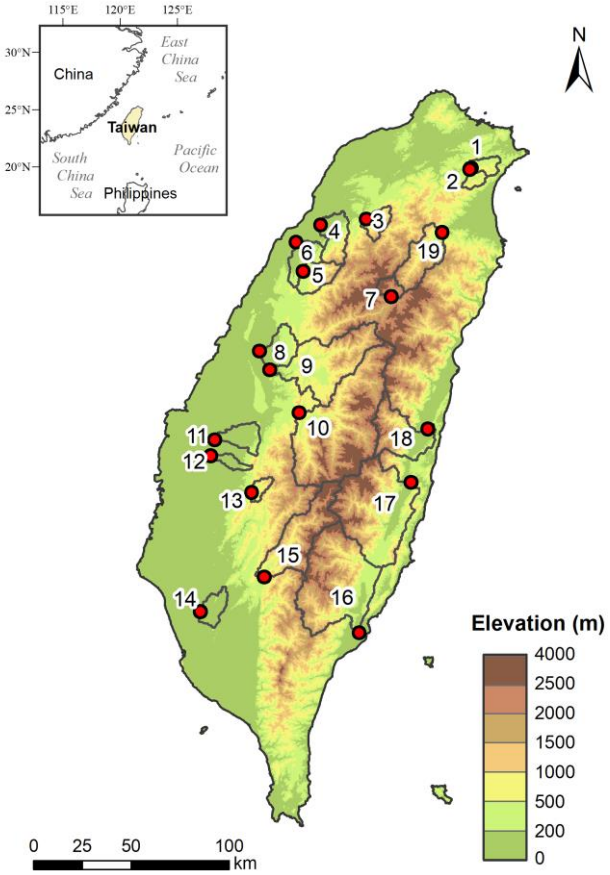

Figure 1: Topographic distribution of Taiwan and the locations of the selected catchments. The catchment ID can be referred to Table S2 and S3, in which the primary descriptions of hydrologic events and landscape variables are listed.

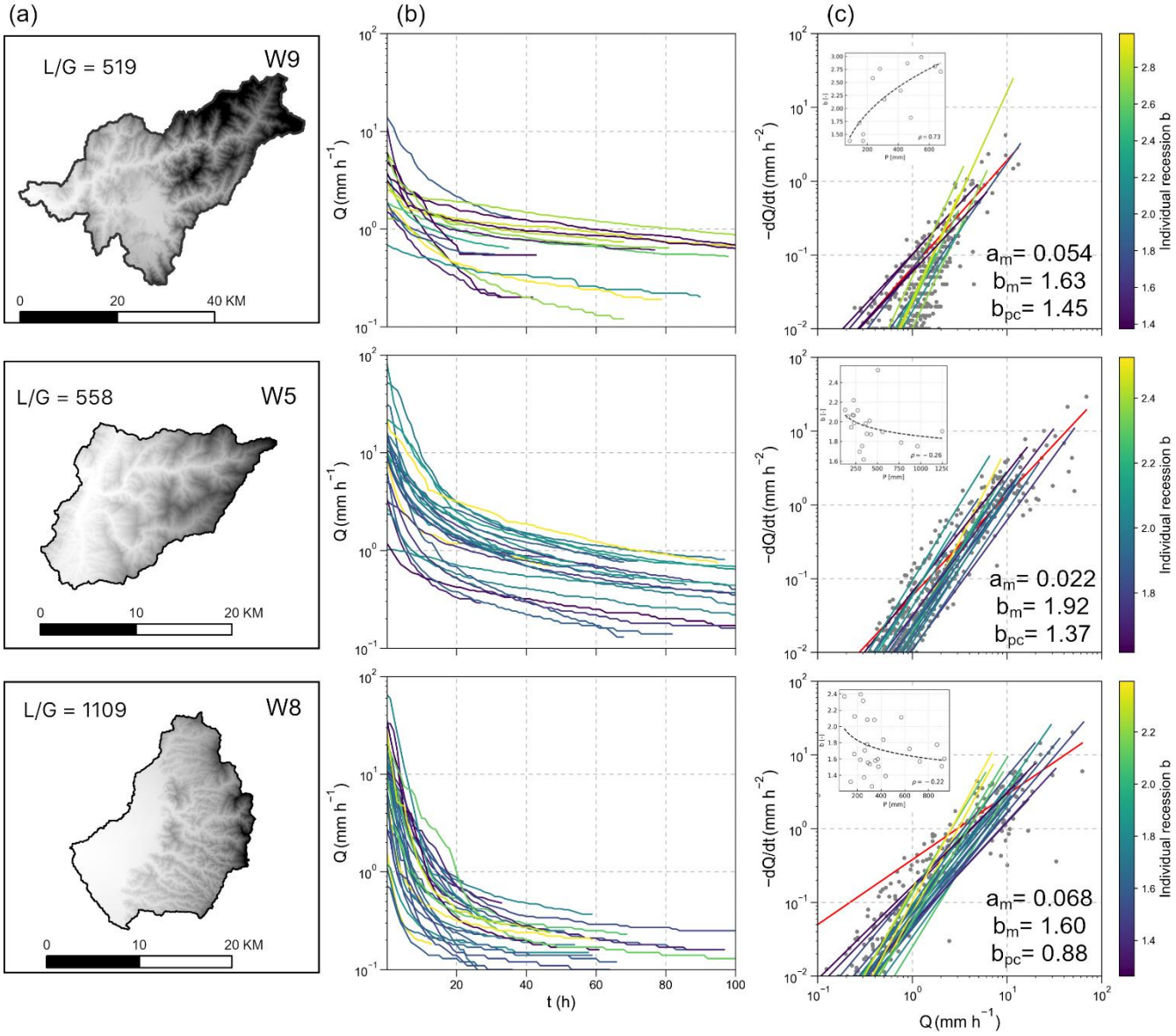

Figure 2: Landscape and recession plots for catchment W9 (row 1), W5 (row 2), and W8 (row 3). Landscape and flow-path topography (L/G) are shown in column (a). The selected recession segments from different rainstorms are shown in (b). Recession plots of all selected rainstorms are shown in column (c). The median of recession parameter *a* and b_m and the b_{pc} derived from the point-cloud are shown in the lower-right corner. The recession *b* from individual segment are colored from purple to yellow with increasing value of *b*.

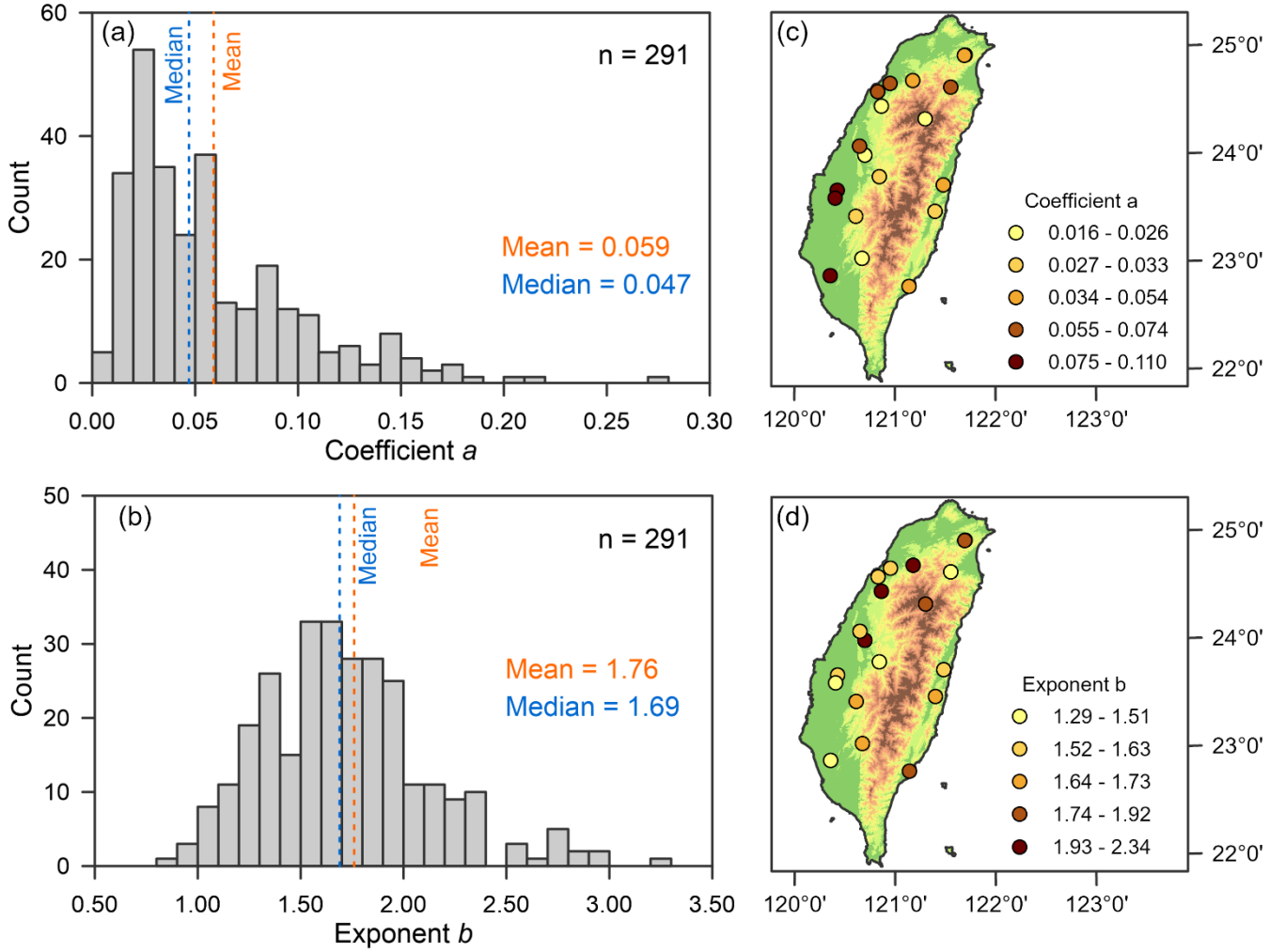

Figure 3: Distributions of recession parameter *a* (a) and *b* (b) in all catchment-events. Spatial distributions of the medians of parameter *a* (c) and *b* (d). Colors of dot represent quantiles category.

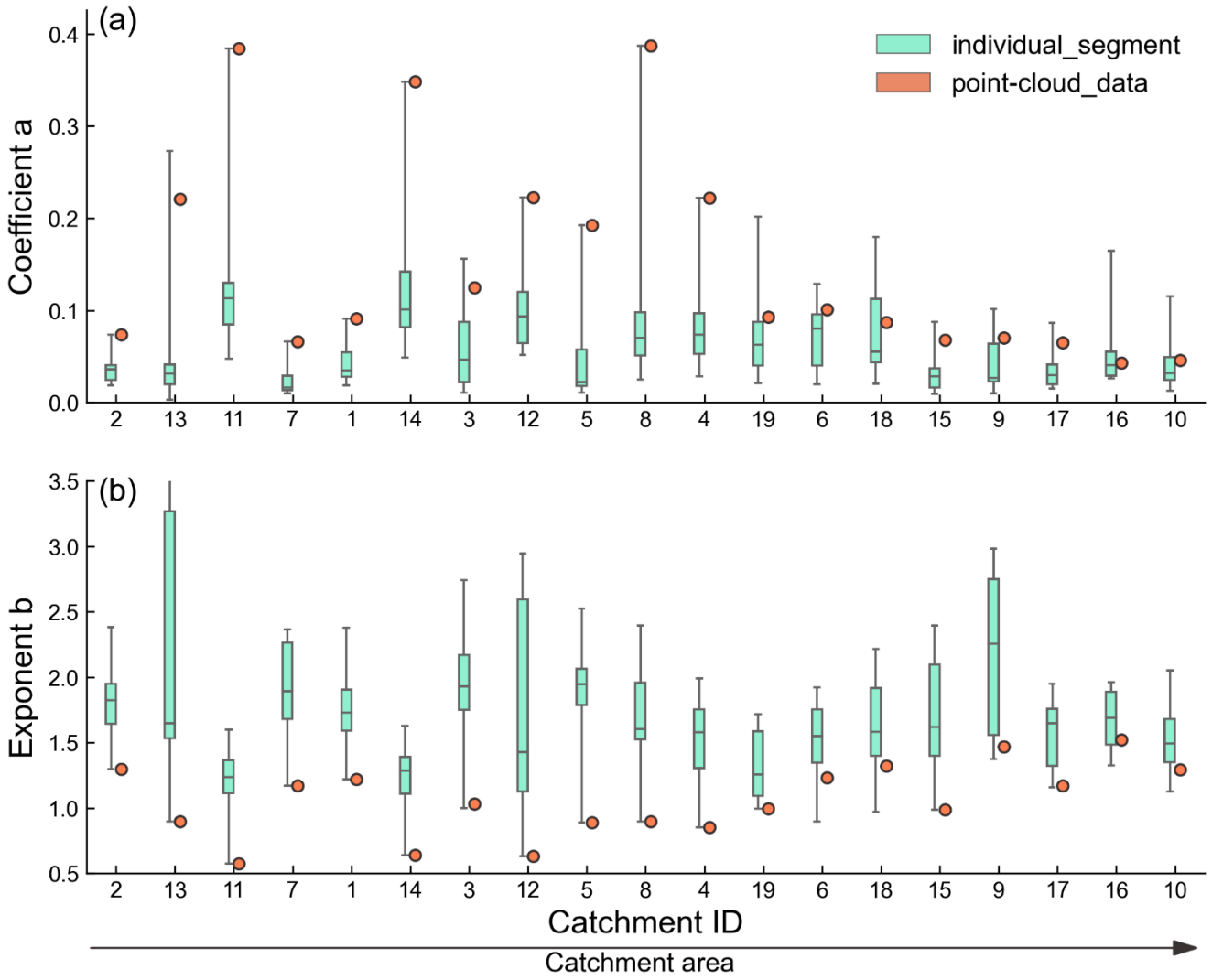

520 **Figure 4: Boxplots of coefficient *a* (a) and exponent *b* (b) derived from individual recession segment (cyan box) and point-cloud data (orange dot). The drainage area is used in *x*-axis in ascending order. Boxes show the interquartile and data range.**

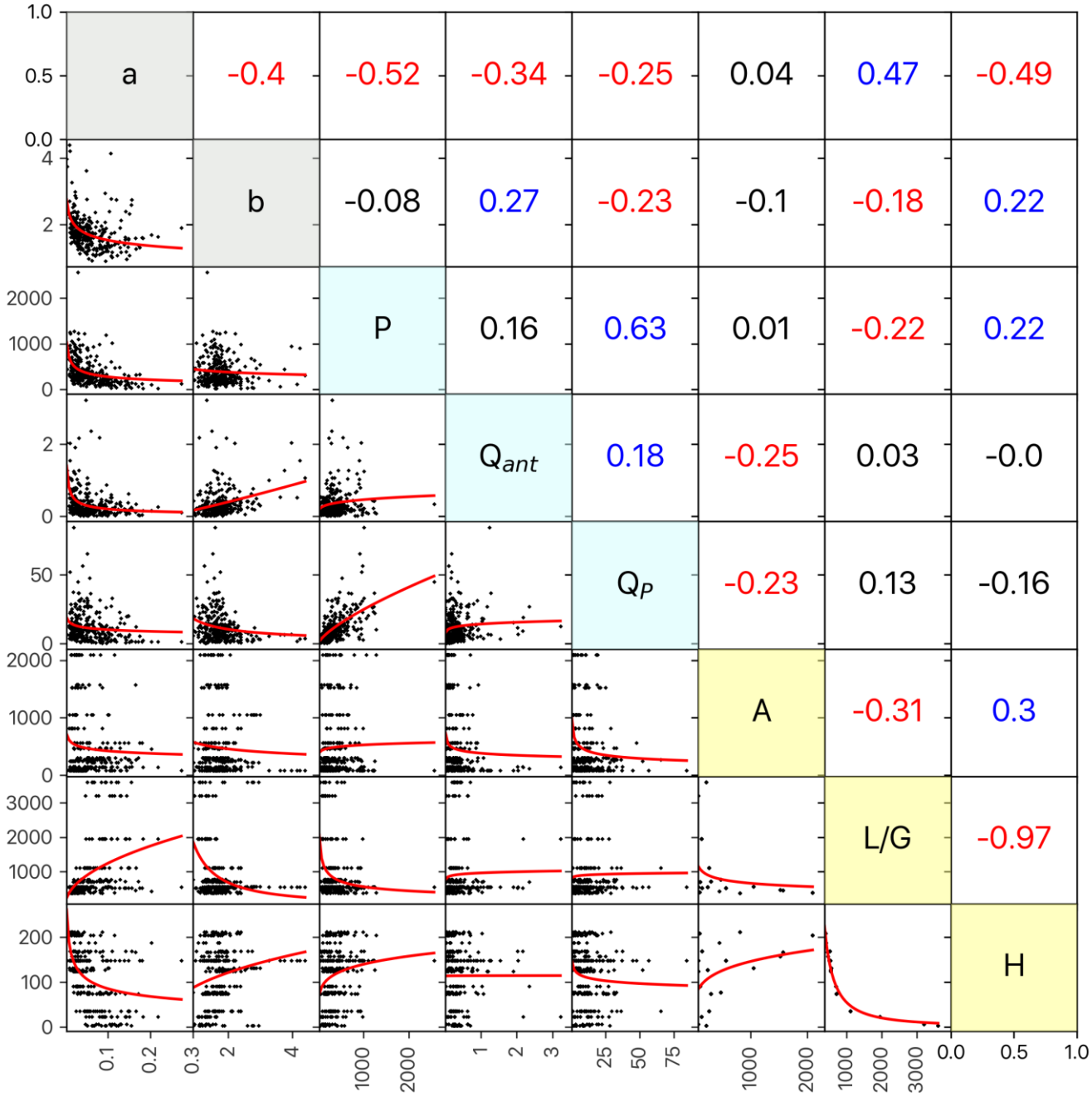

Figure 5: Recession parameter, *a* and *b* against event and landscape variables. Below diagonal: scatter plots for recession parameters with a power-fit regression (red line). Above diagonal: corresponding Spearman correlation coefficients. Values in blue and red color are positive and negative statistically significant with the 95% level of confidence ($p < 0.05$), respectively. Notes that all station and event are shown in this figure.

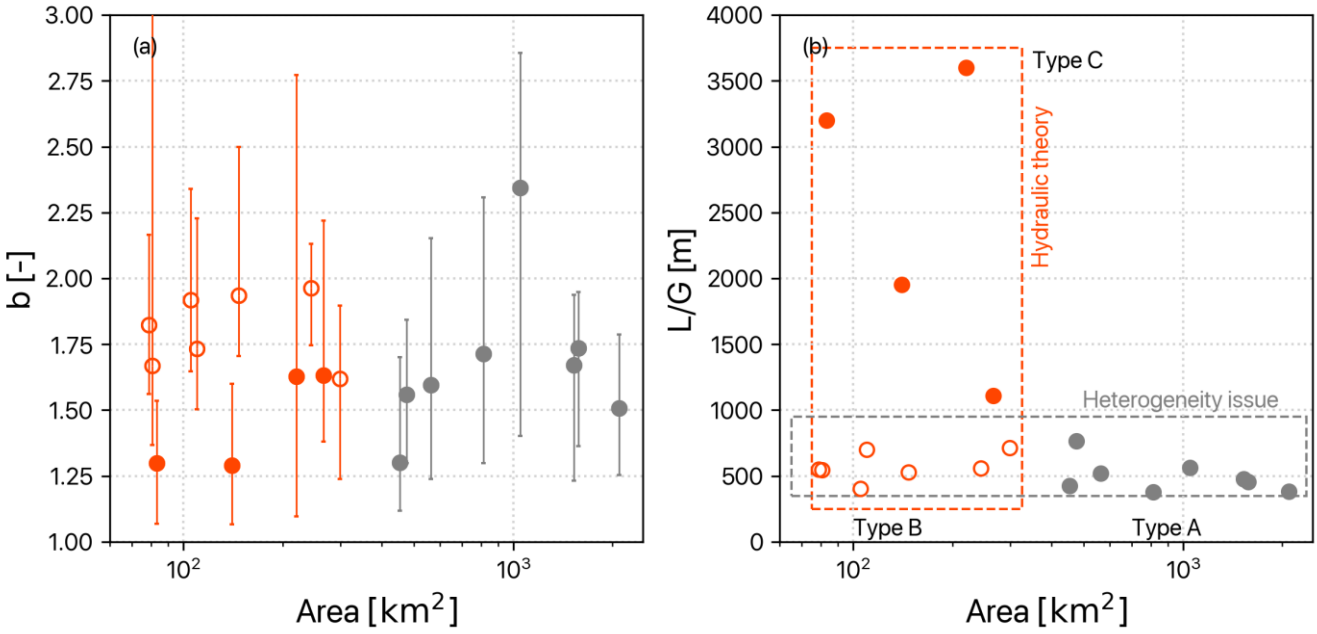

Figure 6: The relationship between drainage area and the recession exponent (a) and the flow path topography (*L*/*G*) (b). The error bar on (a) is the range of the recession exponent of each catchment. The orange and gray dots represent small and large catchments, respectively. The solid and hollow dots represent large and small L/G. The recession behaviors in small and large catchments could be explained from two perspectives in terms of hydraulic theory (orange box) and heterogeneity issues (gray box).

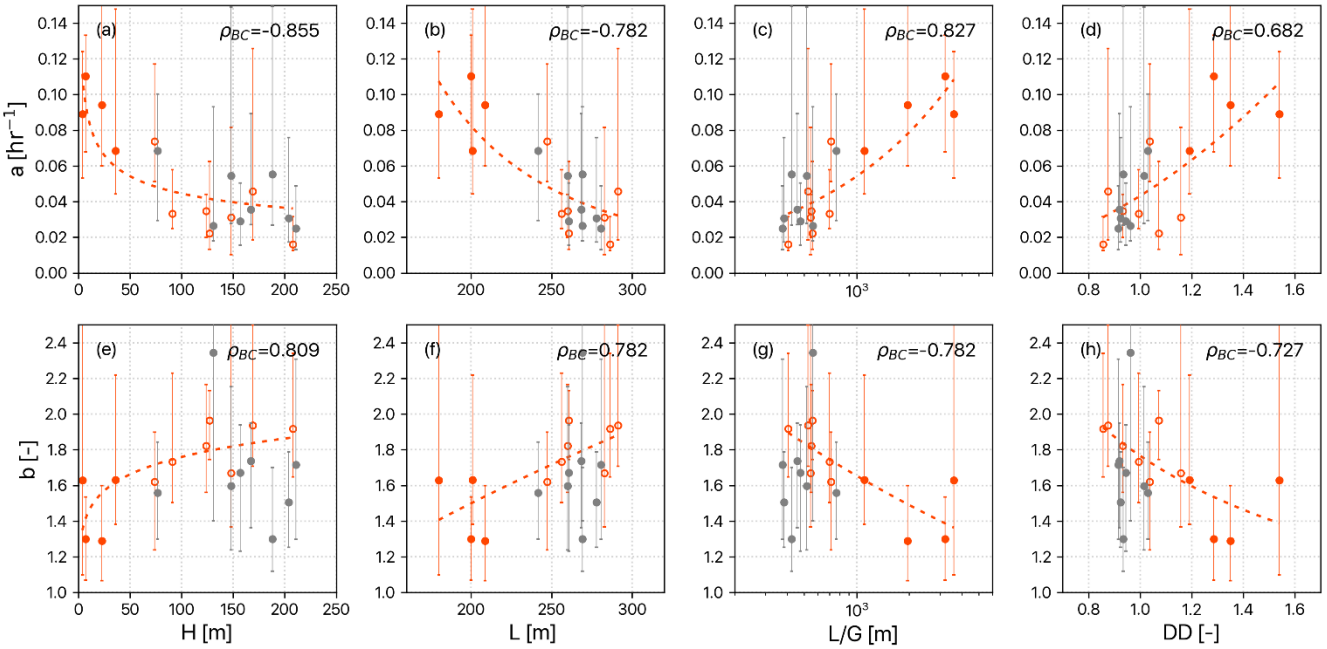

Figure 7: Scatter plots of the median and the range of 10th-90th percentile of recession parameters and landscape variables. gray solid, orange hollow, and orange solid dots are Type A, B, and C basin, respectively. The orange dash line is the power-law fit for small catchments (Type B and C), respectively. The Spearman correlation coefficient (ρ) is listed beside the annotation.

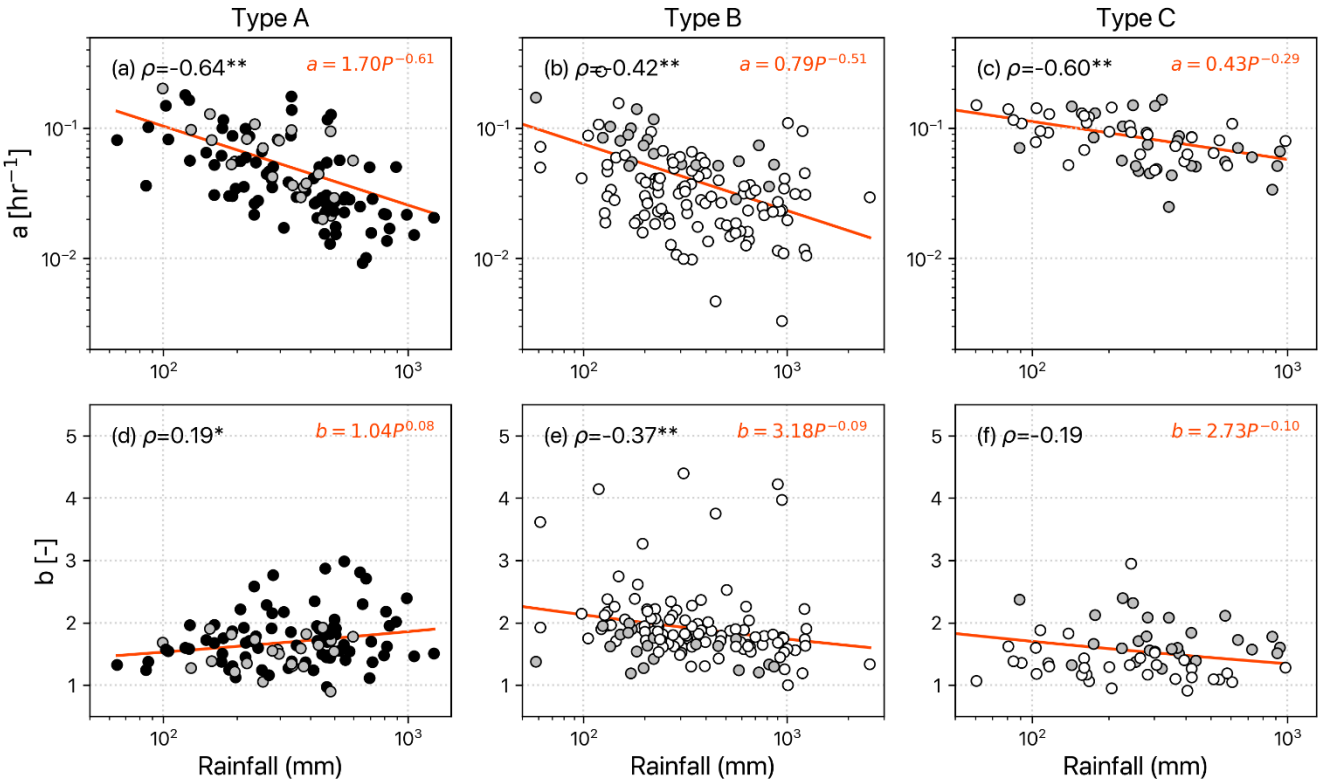

Figure 8: Scatter plots of recession parameters against total rainfall for different catchment types, corresponding to Fig. 6a. Type A is large catchments (area > 500 km^2), B is small catchments with low *L*/*G* ratio, and C is small catchments with high *L*/*G* ratio. The black-gray-white color of dots represents the low to large L/G. The orange line is the power-law fit with spearman correlation coefficients (* and ** means 90% and 99% level of confidence, respectively).

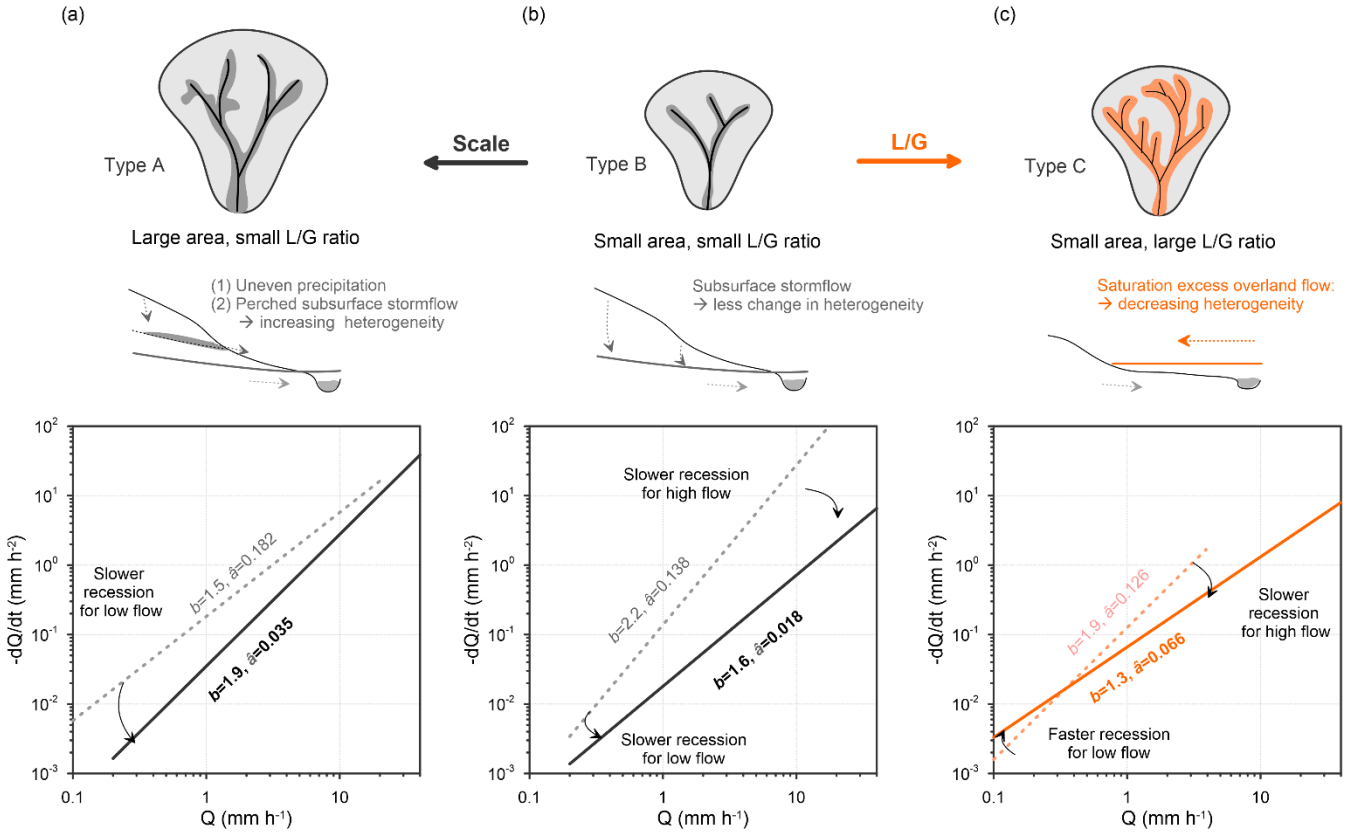

555 **Figure 9: The conceptual diagram demonstrating the regulation of landscape variables on the direction of the rainfall-recession relationship. The top panel presents the drainage area and the stream network of three landscape types of catchment corresponding to Fig. 6b. The middle panel presents the cross-sectional valley with descriptions of drainage behavior. Here, (a) type A, large and steep slope, drains water via multiple sources of subsurface flow; (b) type B, small and steep slope, drains water via fewer sources of subsurface flow; and (c) type C, small and gentle slope, drains via**
560 **the extension of the saturated zone along the riparian zone. Correspondingly, the recession plots for light (dashed line) and heavy (solid line) rainstorms with their recession parameters are presented on the bottom panel.**